Single-Molecule Nanoprobes Explore Defects in Spin-Grown Crystals†

Christopher A. Werley and W. E. Moerner*

Department of Chemistry, Stanford University, Stanford, California 94305-5080

Received: December 29, 2005; In Final Form: March 21, 2006

Thin, platelike single crystals of *p*-terphenyl (PT) doped with terrylene impurity molecules can be prepared by spin-coating from solution. Strikingly, individual terrylene molecules can be observed traveling inside the crystal over distances of several micrometers by using single-molecule fluorescence imaging at room temperature. Analysis of the motion by single-particle tracking and correlation methods indicates that the molecules act as nanoprobes by exploring long, thin crack-like defects with correlated orientations, defects that can be difficult to observe by other means. Apparently, the regions accessible to the moving molecules are in the interior of the crystal and hence are partially protected from oxidation. In addition to the traveling molecules, which photobleach in times on the order of 32 s under continuous irradiation at 2 kW/cm^2, two other spatially fixed populations are observed: one with transition dipole oriented along the *c*-axis of the crystal with a characteristic photobleaching time greater than 32 h, and one with a characteristic photobleaching time of 18 min.

Introduction

The ability to perform optical spectroscopy and microscopy of single molecules in condensed phase samples[1] continues to fascinate scientists in fields ranging from biophysics,[2−5] to cellular biology,[6] to materials and polymer science,[7−9] and even to single-photon sources.[10,11] Information on local interactions can be extracted, molecule by molecule, by the measurement of excited-state lifetimes, spectra, orientations, brightness, degree of energy transfer, and photon correlations, thus removing ensemble averaging and allowing exploration of heterogeneity. Single-molecule studies often show complex statistical fluctuations, which allow useful comparison with theoretical models in a variety of cases.[12−14]

The ability to observe a single molecule at room temperature is often limited by the photobleaching that eventually occurs. For dye molecules, emission of 10^6 photons before photobleaching is typical, and the experimenter must husband these photons carefully to extract the maximum amount of information from the molecule. One materials system with unusual photostability and nearly absent blinking is composed of terrylene (TR) impurities in an organic crystal such as *p*-terphenyl (PT).[15,16] Because terrylene molecules in sublimed *p*-terphenyl can emit over 10^9 photons before photobleaching, this system has been used as a source of single photons on demand (a single-photon source).[17] Indeed, the TR/PT combination has been the subject of significant research in the past due to favorable properties such as high fluorescence count rates (up to 600 000 s^{-1})[18] and a large fluorescence quantum yield (0.9).[19]

Growing and handling micrometer-thick, sublimed crystals of PT doped with TR can be challenging because such thin crystals are susceptible to plastic deformation. Recently, Pfab et al.[20] have implemented an unusual sample preparation method, that of spin-coating doped PT crystals on a flat substrate directly from a solution of PT and TR. Long (>1 day) photobleaching times were reported for single TR molecules in PT crystals prepared in this simple way, opening the possibility for further applications.

In this paper, we confirm the basic results of Pfab et al.[20] and explore the behavior of single TR molecules in spin-grown crystals of PT at room temperature, paying attention to the photobleaching characteristics, and find several different populations of molecules. In addition to extremely stable, stationary molecules, surprisingly, we find that other TR molecules move about inside the crystal, exploring bounded, micrometer-sized defect regions that would be difficult to study by other means. This spatial wandering effect is characterized by single-molecule tracking and correlation analysis. The ability to use single molecules as nanoprobes to explore defects and cracks inside crystals is a novel approach that may find application for the characterization of defects in other condensed phase systems.

Experimental Section

TR was dissolved in solid PT (Aldrich, sublimed) by premelting the two components at temperatures near 200 °C, followed by cooling to room temperature and grinding. A very dilute solid mixture of TR in PT (10^{-8} g/g) was dissolved in spectroscopic-grade toluene to make a solution of concentration 3 mg/mL. Doped PT crystals were produced by spin-coating 20 μL of this solution onto an uncleaned, new Pyrex cover slip (no. 1, VWR Scientific) by using a Headway Research Inc. model EC101DT-R485 spin-coater. The acceleration was set to 5000 rpm/s, and the spin speed was 1000 rpm for 18 s, ramping immediately to 3000 rpm for 2 additional seconds. Various pretreatments of the Pyrex cover slip (plasma etching, base wash, etc.) inhibited reliable formation of large, crystalline regions on the surface, and the best results were obtained with fresh cover slips from the manufacturer. Fluorescence microscopy of control PT samples without the TR dopant revealed only a few single-molecule impurities (<3−5 molecules in a 20 μm × 20 μm area). While a portion of the parameter space of sample preparation was explored, this particular substrate

† Part of the special issue "Robert J. Silbey Festschrift".

* Corresponding author. E-mail: wmoerner@stanford.edu. Telephone: 650-723-1727. Fax: 650-725-0259.

10.1021/jp057570b CCC: $33.50
Published on Web 04/19/2006

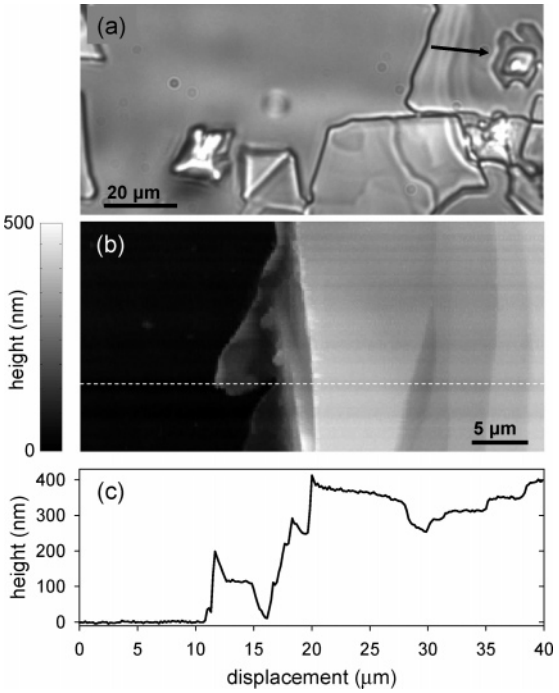

Figure 1. (a) Wide-field, white light image of a large region of glass slide, showing several crystals on the glass surface. Crystal structure is quite varied, with some geometrically shaped crystallites and other less-ordered structures. The arrow indicates an example of crystallite stacking, a common phenomenon. (b) AFM image of (from left to right) glass, crystal edge, and crystal center. A section along the dashed white line, plotted in (c), shows that the crystal rises very abruptly from the smooth surface of the glass slide.

preparation and spin-growth procedure may not be the same as that for Pfab et al.[20]

Single TR molecules in the PT crystals were visualized by using wide-field single-molecule fluorescence microscopy.[21] A 532-nm, diode-pumped, doubled Nd:YAG CW laser from CrystaLaser was used to deliver about 2 kW/cm^2 to the sample by focusing through a 100×, NA = 1.35, oil immersion objective (Olympus Uplan Apo) in an inverted microscope. The laser beam entered the objective off axis so that total internal reflection (TIR) occurred at the *p*-terphenyl/air interface. A detailed description of through-objective TIR microscopy is given by Paige et al.[22] Fluorescence was collected on an Andor Ixon back-illuminated, frame transfer, Si CCD camera with on-chip multiplication gain after removing extraneous laser light with a dichroic mirror (Omega Optical XF2012) and a 590-nm longpass filter. Circularly or linearly polarized light (with any desired orientation) could be sent to the microscope with the appropriate configuration of linear polarizers and a quarter-wave plate in the laser beam path.

Results

Figure 1a shows a white light transmission image of a representative 130 μm × 55 μm area on the glass slide. In all of the samples studied, some crystals had very ordered shapes, particularly diamonds and triangles, while most had irregular boundaries. Crystallite stacking was quite prevalent (an example is highlighted by the arrow in Figure 1a), which made the sample thickness quite variable. The edge of the first crystal plateau was generally quite sharp, typically rising 300−400 nm above the surface of the cover glass (see atomic force microscope images in Figure 1b and c).

At room temperature, PT is a monoclinic platelet-shaped crystal with the extended surface being the (001) (or *ab*) crystal

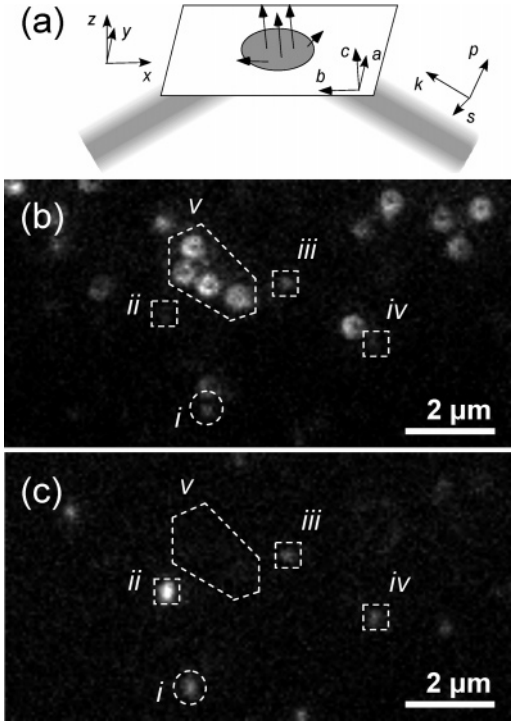

Figure 2. (a) Diagram of the sample and the laser spot during TIR. Black vectors represent terrylene absorption dipoles, which are embedded in the *p*-terphenyl crystal (gray) on the surface of the glass slide. In the bottom two panels, the same sample region is illuminated by (b) *p*-polarized light (field components along the *z* and *x* axes) and (c) *s*-polarized light (parallel to the sample plane, field along the *y* axis only). Molecule i moves in some confined domain. The intensity of this and other moving molecules is in general equal for different laser polarizations. Molecules ii, iii, and iv are fixed. The dipole of ii lies in the sample plane, while the dipoles of iii and iv either rotate or have some intermediate orientation. The molecules in v are fixed with their dipoles oriented perpendicular to the sample plane. The annular "spots" are observed for all *z*-oriented molecules and result from the dipole emission pattern and inherent aberration in the high-index, anisotropic *p*-terphenyl crystal.

plane.[23,24] This has important ramifications because it determines the alignment of TR molecules, known to insert into the lattice with their transition dipoles (which lie along the long axis of the molecule) almost parallel to the *c*-axis.[15] In this orientation, the TR molecular dipole would be perpendicular to the extended surface of the crystal and sample (see Figure 2a). Thus, one might expect to observe only one population of molecules, with the dipole aligned along the optical axis of the microscope (*z*-axis), perpendicular to the sample plane.

Surprisingly, when the sample was continuously irradiated with 532-nm light via TIR, three distinct populations of single molecules were revealed. The first and most unexpected population, described in detail below, was comprised of relatively short-lived, dynamic molecules that jiggled and moved around inside the crystal on the 100-ms time scale (circle in Figure 2). The other two populations had fixed positions but different orientations, as evidenced by the emission patterns and intensity resulting from excitation by different polarizations of light. Figure 2a diagrams the orientation of terrylene absorption dipoles (black vectors in the central oval) and the axis systems used to describe the polarization components of the incoming laser light. All TR molecules are trapped within PT crystal platelets (like those shown in Figure 1) on the top surface of the glass slide. The two immobile populations are easily distinguished when the sample is irradiated with *p*-polarized (Figure 2b) and *s*-polarized (Figure 2c) light.

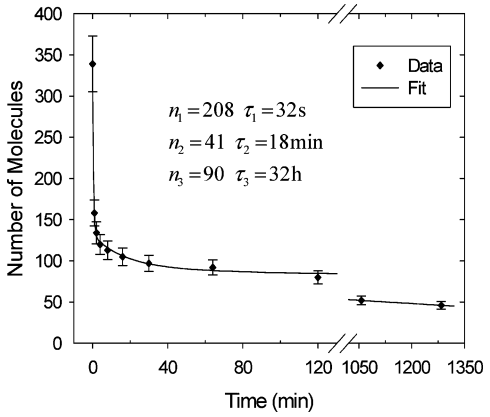

Figure 3. A large number of single molecules under continuous irradiation at 532 nm (circularly polarized, 2 kW/cm^2) were observed to determine the number of surviving, unbleached molecules at different points in time. Error bars represent 10% of the tabulated values, which is approximately the uncertainty in counting. The data are well described by a triple exponential (see eq 1), which implies three populations each with its own characteristic photobleaching time.

Z-oriented molecules (the expected orientation where the TR transition dipole is oriented approximately parallel to the *c*-axis of the molecular crystal) should not interact with *s*-polarized light (no field component along the *z*-axis) but should be strongly excited by *p*-polarized light (primary field component along the *z*-axis). There is a large population displaying this behavior (dashed polygon in Figure 2) and all of these molecules have an annular emission pattern. This "donut"-shaped image has been previously observed on numerous occasions[20,25] and can be explained by inherent aberration of a *z*-oriented emitter in the high-index *p*-terphenyl crystal.[26,27] Molecules in the last population (squares in Figure 2) have a fixed location and an alignment not parallel to the *z*-axis. Some of these have roughly equal intensity for both laser polarizations (molecules iii and iv) and so might be about 45° out of the sample plane or might be rotating, while others fluoresce only with *s*-polarized excitation (molecule ii) and lie almost fully in the plane.

It should be noted that all three populations show single-step photobleaching, identifying them as single molecules. A control in which undoped PT was spin-cast onto an uncleaned slide did show a few single-molecule spots, but in the many regions of crystal explored, neither moving molecules nor annular emission patterns were observed. These facts strongly suggest that the molecules described here (the movers and *z*-aligned molecules) are in fact single TR molecules.

To assess photostability, the number of surviving, unbleached, single molecules $N(t)$ in a crystal was determined as a function of time, while circularly polarized laser irradiation was maintained at a constant intensity of ~2 kW/cm^2 (see Figure 3). The data are best fit by an equation of the form:

$$N(t) = n_1 e^{-t/\tau_1} + n_2 e^{-t/\tau_2} + n_3 e^{-t/\tau_3} \qquad (1)$$

The first term represents a short-lived population ($\tau_1 = 32$ s) and results primarily from the moving molecules, most of which have photobleached by the end of the first minute. In stark contrast to the movers, some of the *z*-oriented molecules are extremely long-lived: 46 of ~180 were still emitting after 21.5 h of constant illumination. The longevity of these molecules leads to the last term in eq 1 ($\tau_3 = 32$ h), and since many did not bleach, this characteristic time should be regarded as a lower limit. These long-lived molecules have the expected crystalline alignment (dipole parallel to the *c*-axis), and their exceptional photostability probably results from the fact that they are substitutionally integrated into the protective crystal matrix. Molecules with this extreme level of stability can be particularly useful in situations where single-molecule emission leads to useful properties, such as antibunching and single-photon emission.[17]

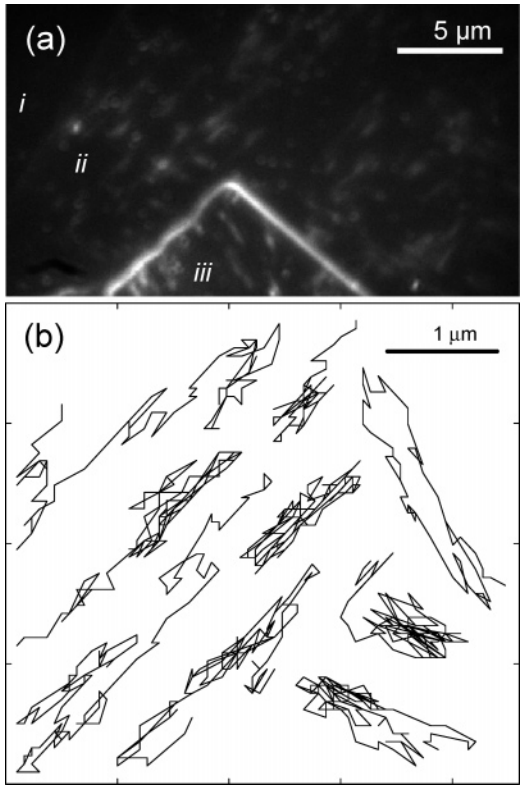

Figure 4. (a) Summation of all 100 frames in a 10-s movie of this sample region irradiated with *s*-polarized, 532-nm light. Region i is just glass, region ii is a large crystal platelet, and region iii is a smaller, higher platelet that appears to rest on ii. Streaks show where moving molecules spend their time as they explore bounded cavities within the crystal. (b) Actual tracks of several moving molecules, traced by hand from frame to frame through the movie. Time between points in the trajectory is 100 ms.

The middle term in eq 1 ($\tau_2 = 18$ min) arises from a combination of both fixed populations. Molecules not aligned along the *z*-axis would be expected to have shorter lifetimes because they are poorly integrated into the PT lattice and thus are vulnerable to photobleaching by free oxygen. *Z*-aligned molecules contributing to the first and middle term must also be relatively unprotected by the crystal lattice, presumably because of their proximity to a crystal surface, defect, or domain boundary.

The remainder of the work focuses on the unusual moving molecules and their environment. Figure 4a is the sum of 100 frames (100 ms/frame) in a 10-s movie of the emission from a sample irradiated with *s*-polarized light. The summing procedure makes Figure 4a effectively a single picture with a 10-s exposure time. Because of this long exposure time, very dim structures/emitters with relatively fixed position that cannot be seen in any individual frame of the movie are apparent in the sum. At the same time, molecules that move around in a constrained region appear as streaks. Three regions are identified in Figure 4a, the bare glass (i), a large region of crystal with a flat surface (ii), and a higher crystal surface (iii) stacked on ii. Crystal edges are easily seen because they scatter fluorescence that is normally trapped in the high-index platelet toward the detector. In many

cases such as the boundary between ii and iii, the edges are quite bright. Donut-shaped emission patterns from *z*-aligned molecules can be observed (although they are quite dim) despite the *s*-polarized excitation light because the absorption dipole is slightly off axis.[20,28] White streaks result from moving molecules whose intensity is spread throughout the region they explored. It is fairly clear that molecules move within some thin and extended cavity or defect, and that the long axes of many of these defects are parallel. This is made clearer in Figure 4b, where the trajectories followed by nine molecules were tracked by hand as the movie (shown in Figure 4a) progressed in 100-ms increments, with accuracy of ~70 nm for each position determination (the pixel size). A movie showing many moving molecules in the presence of many fixed *z*-oriented molecules is available as online Supporting Information.

Analysis and Discussion

The unexpected presence of a large number of moving single molecules is quite fortuitous because they can be used as a probe for defects in the crystal structure. The characteristics and extent of motion yields information on the size of cavities/defects within the crystal and provides clues about the environment in which these molecules are diffusing. One possibility worth considering is that the moving TR molecules are trapped in a solvent-filled cavity in the crystal. As is well-known, the diffusion coefficient of a free particle buffeted by thermal fluctuations in a gas or liquid can be calculated by using the Einstein−Smoluchowski relation, $D = kT/f$, where f is the frictional drag coefficient. For a small, flat molecule such as terrylene diffusing in a large volume of toluene (the solvent in which the *p*-terphenyl was dissolved prior to spin-coating), the diffusion coefficient should be on the order of $D = 400\ \mu m^2/s$. To characterize the diffusion of the moving molecules, we begin with the mean-squared displacement extracted from the single-molecule trajectories,[29] which for unconstrained Brownian motion follows the familiar relation for diffusion in two dimensions $\langle r^2 \rangle = 4Dt$. Mean-squared displacement as a function of time lag, τ, for the tracks in Figure 4b was calculated using:

$$\langle r(\tau)^2 \rangle = \langle (x(t) - x(t+\tau))^2 + (y(t) - y(t+\tau))^2 \rangle \quad (2)$$

where the average is taken over time and all tracks. Two conclusions can immediately be drawn from results plotted in Figure 5a: the diffusion coefficient is much lower than would be expected in solution ($D = 0.08 \pm 0.01\ \mu m^2/s$ for short τ), and movement is clearly constrained (for unconstrained, Brownian diffusion the mean-squared displacement is linear with time; the solid line showing the prediction for constrained motion will be described below).

One method to analyze the asymmetry of a trajectory, as described by Rudnick and Gaspari,[30] is with the radius of gyration tensor, **T**. In two dimensions, this tensor is:

$$\mathbf{T} = \begin{pmatrix} \langle x^2 \rangle - \langle x \rangle^2 & \langle xy \rangle - \langle x \rangle \langle y \rangle \\ \langle xy \rangle - \langle x \rangle \langle y \rangle & \langle y^2 \rangle - \langle y \rangle^2 \end{pmatrix} \quad (3)$$

The eigenvalues of this tensor are R_1^2 and R_2^2, the squares of the principal radii of gyration. These two characteristics of a trajectory are representative of the long and short axis of the motion and can be combined to provide a measure of track asymmetry, the asphericity parameter:

$$A_2 = \frac{(R_1^2 - R_2^2)^2}{(R_1^2 + R_2^2)^2} \quad (4)$$

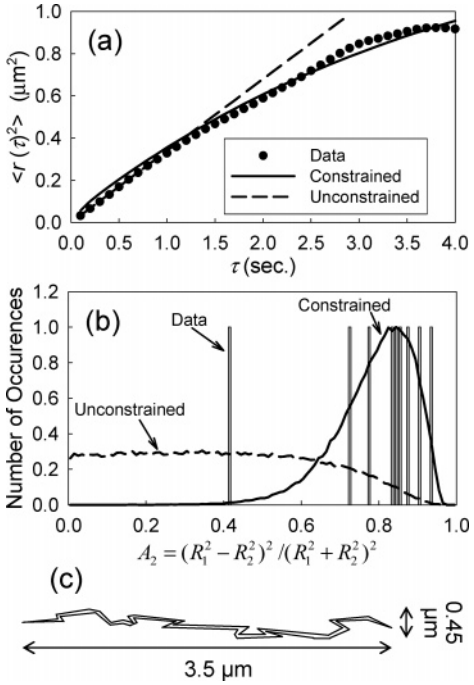

Figure 5. (a) Mean-squared displacement as a function of time lag, τ, between steps. Circles are data, dashed line is the expectation for unconstrained Brownian diffusion (with D calculated from the first few points), and the solid line is the prediction for diffusion constrained in a rectangular region with dimensions $0.45\ \mu m \times 3.5\ \mu m$. (b) Histogram of the asymmetry parameter A_2 (see text). The vertical bars represent values for recorded single-molecule tracks, the dashed line shows the distribution of values for unconstrained Brownian diffusion, and the solid line represents the predicted distribution for molecules trapped in the rectangular domain described above. (c) Schematic of one possible shape for the defects in the crystal. (Not drawn to scale.)

A histogram of A_2, which is 0 for a circular track and 1 for a completely extended, linear track, is plotted in Figure 5b. Gray bars show data values for several single molecules, and the dashed line is a simulated distribution for unconstrained, Brownian diffusion (compare to Saxton[31]). The observed values cluster near 1 because the tracks are quite thin and extended.

To try and unravel the nature of the defect or cavity within which the molecules are moving, diffusion was simulated by generating random walks in a bounded, two-dimensional region with reflective walls. The length, width, and diffusion coefficient were varied in silico until the simulated A_2 histogram and mean-squared displacement plot matched experimental values (solid line in Figure 5a and b). The best values for the variable parameters were $D = 0.19\ \mu m^2/s$ in a $3.5\ \mu m \times 0.45\ \mu m$ box. TR diffusing in a two-dimensional, toluene-filled box with these dimensions would certainly not display the observed behavior; molecules would move much more rapidly. Additionally, faster movement should be observed on short time scales (near $\tau = 0$) before the molecule has had time to explore the boundary in the short dimension. To reconcile this apparent contradiction, we imagine several possibilities. For example, the single TR molecules may be trapped within extremely narrow, jagged cracks, which are not linear (or planar projected into two dimensions) over their entire length. The edges of the box described above would represent the most peripheral points in the trajectory, or worded another way, they represent the largest allowed displacements from the trajectory's center of mass. A depiction of this is given in Figure 5c (note that, in reality, crack width would be much narrower relative to box dimensions). In this model, the effective diffusion coefficient is greatly reduced because a moving molecule can only diffuse a very short

distance without hitting a crystal wall. Exploration of the edge occurs on a much faster time scale than the 100-ms integration time of each frame in the movie and so would not be observable in this experiment. Measured results are consistent with this model: mean-squared displacement will not be sensitive to such fine structure because of the long integration time, and A_2, which is a property of the space explored by the molecule, is a better indicator of the size of the box than a molecule's immediate surroundings. Another possibility might be a planar crack in which the TR molecules do not reflect ballistically from the walls, but rather stick and release on a time scale smaller than our frame update time of 100 ms. In this case, the transverse motion would reflect to the projection of the planar crack onto the two-dimensional focal plane of the microscope.

Additional insight can be gained about molecular motion within the crystal by searching for spatiotemporal correlations within the sequence of images of molecular positions. While technically an ensemble average measurement in that heterogeneity between trajectories is suppressed, this method allows comparison with simple models. From the full stack of images, the complete three-dimensional (x, y, t) correlation was calculated, a method that has recently been applied to biological systems.[32] A 3.4 μm $\times$ 10.7 μm region of crystal containing $\sim$10 moving molecules from the upper part of the image in Figure 4a was chosen for correlation analysis because it displayed relatively uniform mover behavior. A value was determined for average background signal, and this number was subtracted from every frame in the movie. The correlation was calculated by

$$C(\xi, \eta, \tau) = \langle I(x, y, t) I(x + \xi, y + \eta, t + \tau) \rangle \qquad (5)$$

where I is the intensity and $\langle\rangle$ indicates an average over both spatial dimensions and time. The correlation for long times was subtracted from that for short times to remove the effects of stationary, bright objects. The result of this analysis is a new movie of a single bright spot that spreads in time. It should be completely described by the convolution of the point-spread function (PSF) of the microscope and the solution to the diffusion equation for the system being studied.[32] The calculated correlation for $\tau = 0$ and 0.8 s is shown in Figure 6a and d. Sections along the short and long axis are plotted in Figure 6c and f (symbols) as are their Gaussian fits (lines).

Of particular note is the fact that a cross section along the short axis, depicted by triangular symbols, does not broaden significantly with time. This implies that TR molecules have already explored the edges of the crack within the integration time (100 ms) of the first frame. In fact, the distribution along the short axis at $\tau = 0$ is essentially the PSF of the microscope, from which it can be concluded that crack width is thinner than $\sim$200 nm (PSF full width at half-maximum). Because the TR molecules are so constrained along the short axis, for the purposes of this correlation analysis, movement can be modeled as one-dimensional diffusion along the long axis. The convolution of the solution to the one-dimensional, unconstrained diffusion equation (diffusion along the long axis is unconstrained for short times) and the PSF is given by:

$$C(l, s, t) = \frac{1}{2\pi\sigma_{\mathrm{PSF}}\sqrt{(\sigma_{\mathrm{PSF}}{}^2 + 2Dt)}} \exp\left[-\frac{1}{2}\left(\frac{l^2}{(\sigma_{\mathrm{PSF}}{}^2 + 2Dt)} + \frac{s^2}{\sigma_{\mathrm{PSF}}{}^2}\right)\right] \qquad (6)$$

where l (s) is the spatial variable along the long (short) axis,

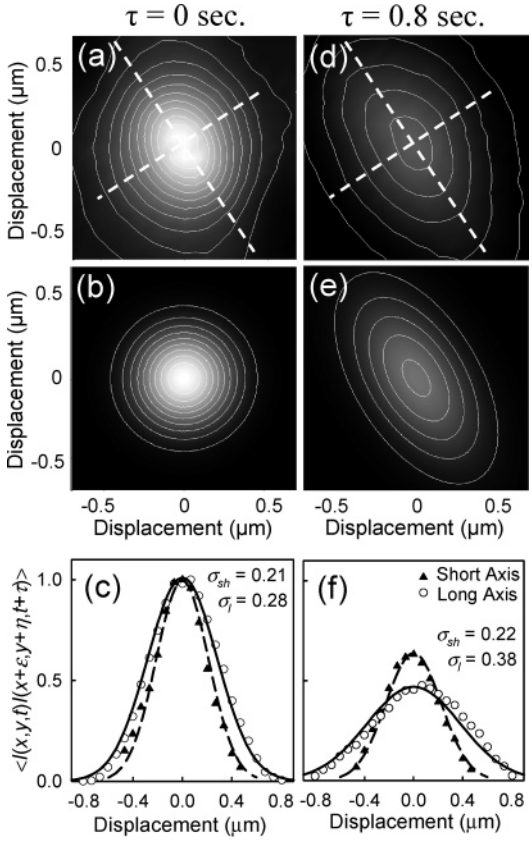

Figure 6. Analysis of the three-dimensional (x, y, t) correlation of molecular position in a small region of crystal, where all movers displayed relatively uniform behavior. Correlation was calculated with eq 5 by using the movie described previously. Panels (a−c) result from autocorrelation ($\tau = 0$), while panels (d−f) were calculated with a time lag $\tau = 0.8$ s. (a) and (d) show calculated correlation, with sections along the dashed white lines given in (c) and (f). Notice that the standard deviation along the short axis, σ_{sh}, remains essentially constant through time, while the standard deviation along the long axis, σ_{l}, increases significantly. (b) and (e) are analytical predictions for one-dimensional diffusion. Intensity along the short axis is determined by the point-spread function of the microscope and intensity along the long axis is given by a convolution of the point-spread function of the microscope and the one-dimensional diffusion equation (eq 6). The diffusion coefficient is determined by fitting the convolved distribution to the actual intensity correlation along the long axis at $\tau = 0.8$ s [circles in (f)].

and σ_{PSF} is the standard deviation of the PSF, approximated by a Gaussian. Fitting this equation to the cross section along the long axis at 0.8 s ($s = 0$, Figure 6f, solid line) yields $D = 0.06 \pm 0.01$ μm^2/s (compare to 0.08 ± 0.01 μm^2/s determined from molecule tracking and the mean-square displacement, a calculation which assumes two-dimensional instead of one-dimensional diffusion). By using this model, predicted forms for $C(l, s, 0)$ and $C(l, s, 0.8)$ are plotted in Figure 6b and e, respectively, where eq 6 has been rotated to match the orientation of the long axis in the data. The biggest difference between observed and predicted values is the asymmetry in Figure 6a, which results from the influence of environmental anisotropy over the 100-ms integration time of the first frame.

Other regions of crystal from different samples showed similar, but different behavior. In some cases, a subset of molecules did not display behavior characteristic of constraint along the long axis before photobleaching. In many samples, there are two clear crystal domains, each with its own set of parallel defects, not an unreasonable possibility considering the propensity of the PT crystal to form microtwins.[33] This is

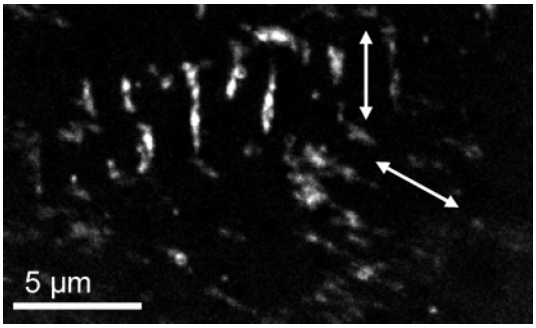

Figure 7. The variance of intensity in time is plotted for each pixel in the time stack of images for this sample. This method highlights pixels that recorded large intensity fluctuations caused by moving, blinking, and/or photobleaching molecules. Two crystal domains with parallel cracks can be seen: one with vertical cracks and one with cracks running from upper left to lower right, as signified by the arrows.

highlighted for the sample shown in Figure 7, where the variance in time of each pixel in the entire movie is plotted, a procedure that accentuates intensity fluctuations from moving, blinking, and/or photobleaching. Individual moving-molecule trajectories appear to explore cracks in both domains, indicating that molecules can pass from one defect to another through the domain boundary.

Summary

Observation of single terrylene molecules in a spin-grown *p*-terphenyl crystal at room temperature has revealed not only a population of extremely photostable molecules with fixed position and orientation, but also a surprising, previously unreported class of moving molecules. The moving molecules explore the confines of defect regions, which are generally long and thin, suggestive of cracks. While the PT crystals, known to be delicate and susceptible to plastic deformation, are never handled, crack-like defects are still generated during the novel spin-coating crystallization procedure. The individual trajectories of single molecules provide information about the shape and character of the crystal defects, information that is hard to obtain by other means. It is hoped that presentation of these data will stimulate further theoretical and experimental study of this unusual system. For example, acquisition of images at higher speeds or nanometer-scale determination of the positions of the single molecules by fitting the PSF in each frame[34] would lead to understanding of defect structures in these samples at much higher temporal and spatial resolution. Another interesting avenue of study would involve perturbing the crystal environment (pressure, temperature, etc.) and observing the effects on molecular movement and defect structure.

Acknowledgment. We warmly thank Adam E. Cohen for advice regarding the data analysis, Stephanie Nishimura for help with diffusion simulations, and Jaesuk Hwang for assistance with experimental procedure development.

Supporting Information Available: Movie showing many moving molecules in the presence of many fixed *z*-oriented molecules (AVI). This material is available free of charge via the Internet at http://pubs.acs.org.

References and Notes

(1) Moerner, W. E.; Orrit, M. *Science* **1999**, *283*, 1670−1675
(2) Weiss, S. *Science* **1999**, *283*, 1670−1675
(3) Lu, H. P. *Acc. Chem. Res.* **2005**, *38*, 557−565.
(4) Zhuang, X.; Rief, M. *Curr. Opin. Struct. Biol.* **2003**, *13*, 88−97.
(5) Rasnik, I.; McKinney, S. A.; Ha, T. *Acc. Chem. Res.* **2005**, *38*, 542−548.
(6) Moerner, W. E. *Trends Anal. Chem.* **2003**, *22*, 544−548.
(7) Cotlet, M.; Masuo, S.; Luo, G.; Hofkens, J.; Van der Auweraer, M.; Verhoeven, J.; Müllen, K.; Xie, X. S.; De Schryver, F. *Proc. Nat. Acad. Sci. U.S.A.* **2004**, *101*, 13343−13348.
(8) Lee, T.-H.; Gonzalez, J. I.; Zheng, J.; Dickson, R. M. *Acc. Chem. Res.* **2005**, *38*, 534−541.
(9) Barbara, P. F.; Gesquiere, A. J.; Park, S.-J.; Lee, Y. J. *Acc. Chem. Res.* **2005**, *38*, 602−610.
(10) Moerner, W. E. *New J. Phys.* **2004**, *6*, 88.
(11) Lounis, B.; Orrit, M. *Rep. Prog. Phys.* **2005**, *68*, 1129−1179.
(12) Jung, Y.-J.; Barkai, E.; Silbey, R. J. *J. Chem. Phys.* **2002**, *117*, 10980−10995
(13) Barkai, E.; Jung, Y.-J.; Silbey, R. J. *Annu. Rev. Phys. Chem.* **2004**, *55*, 457−507.
(14) Hummer, G.; Szabo, A. *Acc. Chem. Res.* **2005**, *38*, 504−513.
(15) Kummer, S.; Kulzer, F.; Kettner, R.; Basché, Th.; Tietz, C.; Glowatz, C.; Kryschi, C. *J. Chem. Phys.* **1997**, *107*, 7673−7684.
(16) Kulzer, F.; Koberling, F.; Christ, Th.; Mews, A.; Basché, Th. *Chem. Phys.* **1999**, *247*, 23−34.
(17) Lounis, B.; Moerner, W. E. *Nature* **2000**, *407*, 491−493.
(18) Kummer, S.; Basché, Th.; Bräuchle, C. *Chem. Phys. Lett.*, **1994**, *229*, 309−316.
(19) Durand, Y.; Bloess, A.; Köhler, J.; Groenen, E.; Schmidt, J. *J. Chem. Phys.* **2001**, *114*, 6843−6850.
(20) Pfab, R. J.; Zimmermann, J.; Hettich, C.; Gerhardt, I.; Renn, A.; Sandoghdar, V. *Chem. Phys. Lett.* **2004**, *387*, 490−495.
(21) Moerner, W. E.; Fromm, D. P. *Rev. Sci. Instrum.* **2003**, *74*, 3597−3619.
(22) Paige, M. F.; Bjerneld, E. J.; Moerner, W. E. *Single Mol.* **2001**, *2*, 191−201.
(23) Rietveld, H. M.; Maslen, E. N.; Clews, C. J. B. *Acta Crystallogr. B* **1970**, *26*, 693.
(24) Williams, J. O. *J. Chem Soc. A (London)* **1970**, 2939−2943.
(25) Mehta, A.; Kumar, P.; Dadmun, M. D.; Zheng, J.; Dickson, R. M.; Thundat, T.; Sumpter, B. G.; Barnes, M. D. *Nano Lett.* **2003**, *3*, 603.
(26) Dickson, R. M.; Norris, D. J.; Moerner, W. E. *Phys. Rev. Lett.* **1998**, *81*, 5322.
(27) Böhmer, M.; Enderlein, J. *J. Opt. Soc. Am.* **2003**, *20*, 554.
(28) Bordat, P.; Brown, R. *J. Chem. Phys.* **2002**, *116*, 229.
(29) Vrljic, M.; Nishimura, S. Y.; Brasselet, S.; Moerner, W. E.; McConnell, H. M. *Biophys. J.* **2002**, *83*, 2681−2692.
(30) Rudnick, J.; Gaspari, G. *Science* **1987**, *237*, 384.
(31) Saxton, M. *Biophys. J.* **1993**, *64*, 1766.
(32) Hebert, B.; Costantino, S.; Wiseman, P. *Biophys. J.* **2005**, *88*, 3601.
(33) Williams, J. O. *Chem. Phys. Lett.* **1976**, *42*, 171−173.
(34) Thompson, R. E.; Larson, D. R.; Webb, W. W. *Biophys. J.* **2002**, *82*, 2775−2783.